Transmission System Fault Location Using Limited Number of Synchronized Recorders

Mert Korkalı and Ali Abur
Department of Electrical and Computer Engineering
Northeastern University
Boston, MA 02115-5000 U.S.A.
Email: {mkorkali, abur}@ece.neu.edu

***Abstract*—This paper delineates a new fault location algorithm for meshed transmission networks based on the arrival time differences of traveling waves propagating from the fault point to sparsely and remotely placed synchronized monitoring instruments on particular substations. In fact, it is shown that the fault location can be accurately estimated by taking advantage of the wave arrival delays of a fault transient with regard to a recorder location where the first burst of traveling waves is observed. The technique to be introduced makes use of only available recorders scattered throughout the network. Specifically, the captured waveforms are processed together in order to identify the exact location of the fault under study. The performance of the developed methodology is demonstrated using ATP simulations of fault transients, which are then processed via the MATLAB Wavelet Toolbox.**

***Index Terms*—Electromagnetic transient analysis, fault location, traveling waves, wavelet transform, synchronized measurements.**

I. Introduction

ACCURATE estimation of fault location is an important task for utilities in order to rapidly restore service to their customers. Fault location on transmission and distribution networks remains a challenging problem as the systems continue to change in size and complexity. Availability of synchronized measurements along with computational capabilities in substations allows the use of unconventional methods such as those based on traveling waves for fault location.

The idea of using discrete wavelet transform (DWT) of modal components of the traveling waves initiated by faults, in order to estimate the fault location is first proposed and associated algorithm is presented in [1]. This fault location technique is later applied to the three-terminal (teed) transmission networks in [2]. Also, various two- and three-terminal fault location algorithms have been proposed by several researchers. Nagasawa *et al.* [3] utilize the postfault current differentials at line terminals in order to locate the fault in multiterminal transmission lines by performing a reduction from an n-terminal to a three-terminal system. Reference [4] uses voltage and current phasors offering techniques to eliminate synchronization errors. In [5], the postfault synchronized phasor measurements at different terminals of the multiterminal line are employed for the determination of the fault location. The extensions of these methods for the two- and three-terminal circuits have recently taken place in multiterminal transmission lines and interconnected networks. Indeed, the efforts to accurately estimate the fault location in multiterminal lines have resulted in various fault location schemes. For instance, in [6], synchronized voltage measurements at each end of the line are utilized to locate the fault. In the meantime, Lien *et al.* [7] presented a fault location scheme taking network observability into account. In fact, the authors introduced a method provided that every line section in the network requires one-sided PMU installation. More recently, a generalized fault section selector, as well as fault locator, is proposed by Liu *et al.* [8] for multiterminal transmission lines based on synchronized phasor measurement units.

The authors of [9] introduce a procedure in which the fault-induced transients are processed by means of pattern matching. To estimate the fault area, the distinguishing characteristics of recorded fault waveforms are then utilized to correlate with numerous extracted representative faults. In generating representative patterns, several faults are simulated at certain locations. Despite being an offline procedure, generation of representative features implicates an inadmissible computational cost, thus necessitating an alternative procedure with much less computational cost.

In this paper, arrival time differences of signals from the fault point to the synchronized monitoring instruments are used in order to accurately locate faults. Indeed, at the time fault occurs, electromagnetic waves originated at the fault point travel along neighboring transmission lines. Since these traveling waves follow different paths, they arrive at remote recorder locations with distinct time delays. Referring to these wave arrival delays of a certain fault transient at various locations in the network, the fault location can be determined. The proposed methods generically assume either a single recorder at one end of the faulted line, or a pair of synchronized recorders at both ends of the faulted line. Nevertheless, the technique to be introduced in this paper takes advantage of available recorders dispersed throughout the network as assumed in an earlier work [9]. Particularly, the captured waveforms are processed together in order to identify the exact location of the fault under study. Thus, the proposed method can be considered as a wide-area measurement-based solution to fault location.

The remainder of this paper is organized as follows. Section II of this paper describes the developed fault location algorithm used in identification of the fault occurrence point. Section III

presents the simulation results for a particular fault scenario in the studied network. Finally, Section IV concludes the paper.

II. Description of Fault Location Procedure

In this section, the principal steps establishing the fault location technique are briefly discussed. In order to estimate the fault point precisely, the measured voltage waveforms are initially converted to their modal components using Clarke's real transformation matrix [10] since all transmission line models are assumed to be fully transposed. Then, the modal components are processed through the discrete wavelet transform (DWT) and the squares of the wavelet transform coefficients (WTC^{2}s) are retrieved and employed to detect the fault incipience instant at which signal energy reaches its first local maximum. During the course of simulations, Daubechies-8 mother wavelet [11] with the level-4 approximation coefficients is chosen for the wavelet transformation. At the same time, aerial mode voltage WTC^{2}s in scale-1 have formed a basis for the fault location computations.

Knowing the lengths and electrical characteristics of all transmission lines in the power network, one can calculate the wave propagation time for each transmission line using

$$\tau \triangleq \frac{\ell}{\nu} \triangleq \ell\sqrt{L'C'}, \tag{1}$$

where ℓ represents the line length and ν is the traveling wave velocity; L' and C' designate the per-unit-length inductance and capacitance of the line, respectively.

Consider the case where synchronized recorders are placed at Buses a, b, c, d, and e and a fault occurs at Bus f. Further, suppose that the recorder at Bus a receives the fault-initiated transients first and others receive them later, so that the following times are recorded:

$$\boldsymbol{\mathcal{T}}_{\mathbf{meas}} = \begin{bmatrix} T_{b,a}^{(m)} & T_{c,a}^{(m)} & T_{d,a}^{(m)} & T_{e,a}^{(m)} \end{bmatrix}^{\mathrm{T}}, \tag{2}$$

where $T_{b,a}^{(m)}$, $T_{c,a}^{(m)}$, $T_{d,a}^{(m)}$, and $T_{e,a}^{(m)}$ represent the measured arrival delays of fault signals with respect to the signal received at Bus a. As an illustration, $T_{b,a}^{(m)}$ corresponds to the time difference between the traveling wave times from Buses a and b to the fault point f, or, explicitly,

$$T_{b,a}^{(m)} = T_{b,f}^{(m)} - T_{a,f}^{(m)}. \tag{3}$$

However, since we do not have any knowledge of the fault occurrence point, it is impossible to identify the arrival delays with respect to the fault point f. Instead, the difference between the wave arrival delays $T_{a,f}^{(m)}$ and $T_{b,f}^{(m)}$, designated by $T_{b,a}^{(m)}$, can be measured, provided that the recorders are time-synchronized. Indeed, these time delays can be easily computed for a given system due to the fact that the traveling waves caused by the fault always propagate along the transmission lines following the shortest path rule. Thus, the following vector of time differences resulting from the shortest travel times can be created:

$$\widehat{\boldsymbol{\mathcal{T}}}_{\boldsymbol{x}} = \begin{bmatrix} \tau_{b,x} - \tau_{a,x} \\ \tau_{c,x} - \tau_{a,x} \\ \tau_{d,x} - \tau_{a,x} \\ \tau_{e,x} - \tau_{a,x} \end{bmatrix}. \tag{4}$$

Simplifying the notation in (4), we obtain

$$\widehat{\boldsymbol{\mathcal{T}}}_{\boldsymbol{x}} = \begin{bmatrix} \tau_{ba,x} & \tau_{ca,x} & \tau_{da,x} & \tau_{ea,x} \end{bmatrix}^{\mathrm{T}}, \tag{5}$$

where x refers to any bus in the corresponding power system; $\tau_{a,x}$, $\tau_{b,x}$, $\tau_{c,x}$, $\tau_{d,x}$, and $\tau_{e,x}$ are the calculated shortest travel times from Buses a, b, c, d, and e to Bus x, respectively. The shortest travel time for each bus pair is calculated utilizing the well-known Dijkstra's algorithm [12] recognizing the fact that power networks can be thought of as real-weighted undirected graphs. It should be noted that these computations need to be carried out only once for a given topology. If the topology changes due to any line switching, these calculations will have to be repeated.

Now, a new time difference will be defined as follows:

$$\Delta\boldsymbol{\mathcal{T}}_{\boldsymbol{x}} = \boldsymbol{\mathcal{T}}_{\mathbf{meas}}^{\mathbf{T}} - \widehat{\boldsymbol{\mathcal{T}}}_{\boldsymbol{x}}^{\mathbf{T}}. \tag{6}$$

Here, $\Delta\boldsymbol{\mathcal{T}}_{\boldsymbol{x}}$ can be conveniently used to estimate the fault point since it will be used to match the measured time differences obtained via synchronized recordings with the calculated shortest travel times between each of the fault recorder points. If the fault occurs, say, at Bus x, then by checking $\Delta\boldsymbol{\mathcal{T}}_{\boldsymbol{x}}$ for different x locations (buses) and selecting the one that yields a vector, the ℓ_1-norm of which is minimum among all vectors will provide the solution, i.e.,

$$F_x = \min(\|\Delta\boldsymbol{\mathcal{T}}_{\boldsymbol{x}}\|_1;\ x \in \{1, \cdots, N\}), \tag{7}$$

where x represents the faulted bus, F_x is the minimum norm associated with Bus x, and N denotes the number of buses in the system.

As described previously, the proposed fault location scheme assumes that faults occur only at system buses. However, this assumption is not realistic, for faults are more likely to occur on the transmission lines rather than right at a system bus. Accordingly, a more realistic formulation should be devised in order to locate faults occurring at arbitrary locations along transmission lines.

A two-step methodology is suggested for this purpose. Initial phase is similar to the formulation mentioned above, where faults are assumed to occur only at system buses. However, instead of declaring the faulted bus based on the minimum norm solution, two buses will be selected, where these will correspond to the minimum two values among the ℓ_1-normed difference vectors $\|\Delta\boldsymbol{\mathcal{T}}_{\boldsymbol{x}}\|_1$ in (7), such that

$$\begin{aligned}(F_y, F_z) = \min \big((&\|\Delta\boldsymbol{\mathcal{T}}_{\boldsymbol{y}}\|_1, \|\Delta\boldsymbol{\mathcal{T}}_{\boldsymbol{z}}\|_1); \\ &y \in \{1, \cdots, N\},\ z \in \{1, \cdots, N\} - \{y\} \big).\end{aligned} \tag{8}$$

Subsequently, the pair of buses yielded by (8), will be regarded as two most likely faulted line terminals. Checking if the two potential terminals have a direct link to each other in the studied network, the fault can be declared to have occurred on the line connecting these two terminals. Otherwise, it will be concluded that the fault has taken place on any one of

the lines, incident to one of the two suspect buses. In light of this knowledge, the size of the search space for possible locations is reduced considerably. In this context, if a fault occurs somewhere on a certain transmission line, one way to reliably detect fault location is to "thin-slice" the most likely transmission line(s) by length of certain number, say, the greatest common divisor (*gcd*) of the transmission line lengths in the network. Strictly speaking, the transmission lines, which are incident to the two suspect buses, can be partitioned into equally-separated sections in order to create multiple virtual buses. After processing the same fault location algorithm, a bus location, which best corresponds to a fault point, will be chosen among these fictitious buses. Location of the fictitious bus will then be used to compute the distance of the fault from the nearest substation at either end of the line.

III. Simulation Results

Fault recorders at present typically operate at a high sampling frequency, which is up to 20 kHz. Taking this fact into account, all simulations are carried out in ATP-EMTP program and MATLAB with a sampling frequency, f_s, of 20 kHz corresponding to a sampling time interval of 50 μsec. The fault occurrence time is chosen as 20 msec. The tower configuration of transmission lines is given in [2]. Transmission lines represented by the frequency-dependent models are utilized throughout the simulations. Furthermore, all line segments are assumed to be fully transposed. The aerial mode propagation velocity in scale-1 is calculated as 1.85882×10^5 mi/sec. The studied system is simulated under single-line-to-ground (SLG) faults along various line segments. Line segment lengths, along with wave propagation times, are provided in Table I. Simulation results for SLG fault on the line segment 4–7 with a very small fault resistance ($R_f = 0.1$ mΩ) are presented.

TABLE I
Line Segment Lengths and Wave Propagation Times for the System under Study

Line	Length (mi)	Time (μsec)	Line	Length (mi)	Time (μsec)
$1-2$	130	699.37	$6-11$	145	780.06
$1-5$	75	403.48	$6-12$	55	295.89
$2-3$	115	618.67	$6-13$	30	161.39
$2-4$	85	457.28	$7-8$	125	672.47
$2-5$	145	780.06	$7-9$	45	242.09
$3-4$	90	484.18	$9-10$	165	887.66
$4-5$	110	591.77	$9-14$	150	806.96
$4-7$	280	1506.33	$10-11$	95	511.08
$4-9$	170	914.56	$12-13$	80	430.38
$5-6$	65	349.68	$13-14$	175	941.46

As an example, consider the modified IEEE 14-bus system whose single-line diagram is depicted in Fig. 1. Assume that synchronized recorders exist at Buses 2, 6, 8, 9, and 13. Let there be a fault occurring 150 miles away from Bus 4 on a 280-mile-long line connecting the Buses 4 and 7. Meanwhile, the three-phase synchronized measurements of voltages are assumed to be available as shown in Figs. 2-6. Then, aerial mode WTC^{2}s for each modal voltage are obtained following the decoupling of the phase quantities into the modal voltages.

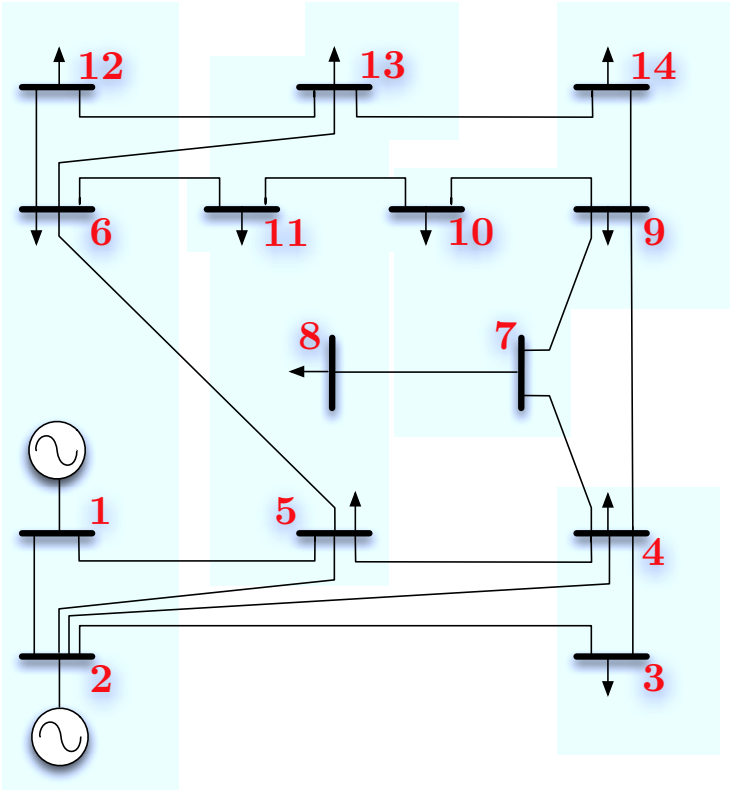

Fig. 1. Single-line diagram of the modified IEEE 14-bus system.

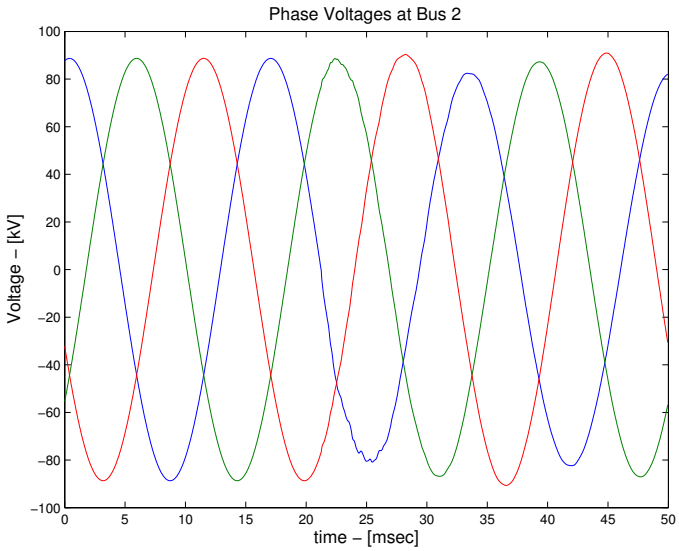

Fig. 2. Faulted phase voltages at Bus 2 for the studied fault.

The WTC^{2}s of the aerial mode voltages are shown in Figs. 7-11. After comparing the local peaks corresponding to each bus, the first local peak observed belongs to Bus 9; hence, the following times in milliseconds are stored in the vector $\boldsymbol{t}$:

$$\begin{aligned}\boldsymbol{t} &= [t_2,\ t_6,\ t_8,\ t_9,\ t_{13}] \\ &= [21.3000,\ 21.8000,\ 21.4000,\ 21.0000,\ 22.0000]\,,\end{aligned}$$

where t_2, t_6, t_8, t_9, and t_{13} are the instants when the first local peaks are detected via the synchronized recorders on

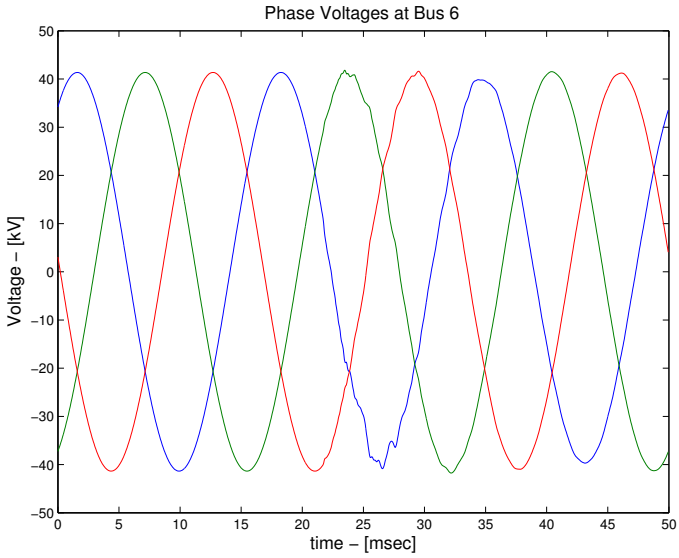

Fig. 3. Faulted phase voltages at Bus 6 for the studied fault.

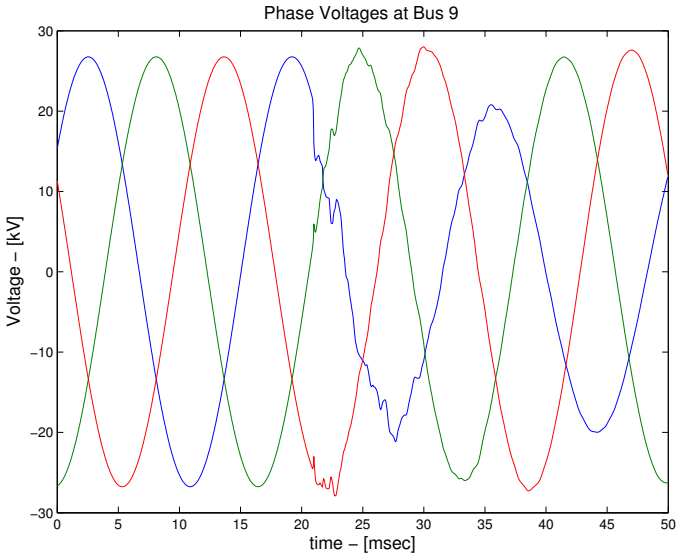

Fig. 5. Faulted phase voltages at Bus 9 for the studied fault.

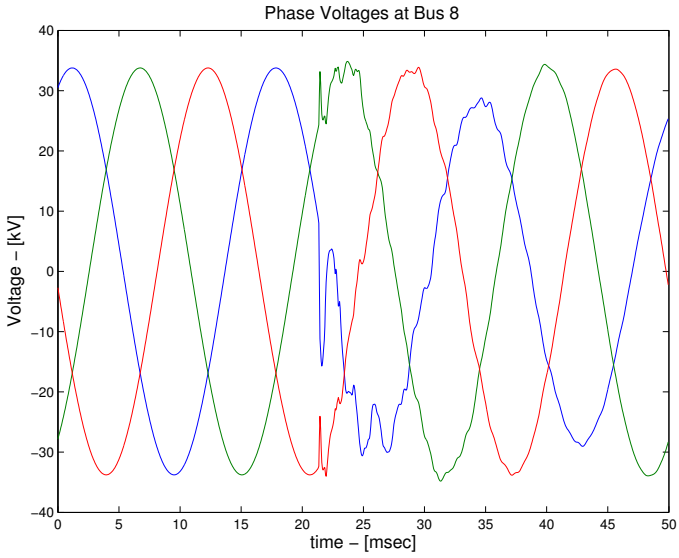

Fig. 4. Faulted phase voltages at Bus 8 for the studied fault.

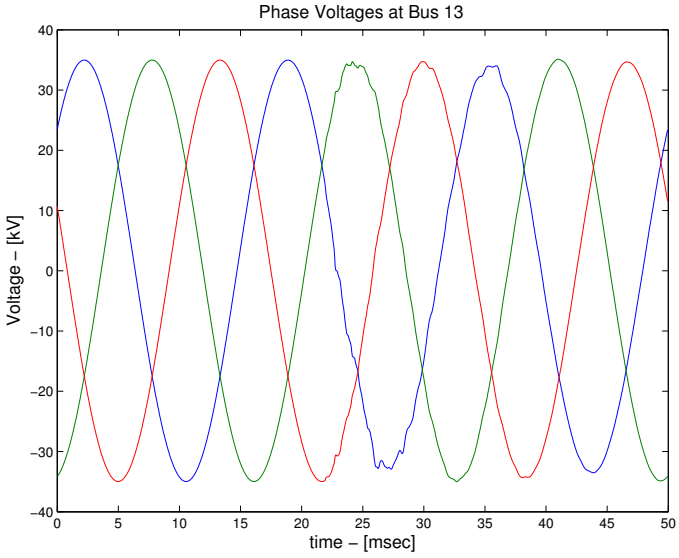

Fig. 6. Faulted phase voltages at Bus 13 for the studied fault.

the respective buses. Since Bus 9 receives the first peak, the arrival delays of fault signals can be computed with respect to the signal received at Bus 9, such that

$$\begin{aligned}\boldsymbol{\mathcal{T}}_{\mathbf{meas}} &= \left[T_{2,9}^{(m)} \;\; T_{6,9}^{(m)} \;\; T_{8,9}^{(m)} \;\; T_{13,9}^{(m)}\right]^{\mathrm{T}} \\ &= \left[0.3000,\ 0.8000,\ 0.4000,\ 1.0000\right]^{\mathrm{T}}.\end{aligned}$$

For the sake of simplicity, all the transmission line configurations are assumed to be identical in order to avoid the differences in traveling wave velocities for each transmission line. However, the proposed method is evidently applicable to power systems with varying line configurations since travel times are defined by (1) and traveling wave velocities can be extracted based on the type and configuration of lines. In this respect, the theoretical shortest travel time differences between any Bus x and Buses 2, 6, 8, 9, and 13 are computed based on the Dijkstra's algorithm as shown below:

$$\widehat{\boldsymbol{\mathcal{T}}}_{\boldsymbol{x}} = \begin{bmatrix} \tau_{2,x} - \tau_{9,x} \\ \tau_{6,x} - \tau_{9,x} \\ \tau_{8,x} - \tau_{9,x} \\ \tau_{13,x} - \tau_{9,x} \end{bmatrix}.$$

Referring back to (8), the most likely terminal pair is found to be $(y, z) = (4, 10)$. Since Buses 4 and 10 do not have a direct connection to each other, it is concluded that the fault should have occurred on one of the lines incident to these terminals. Following the proposed scheme, all seven transmission lines are partitioned into 5-mile sections in order to create new fictitious buses on the system; thus, the network becomes a 206-bus system. The proposed fault location method identifies the faulted node as 131^{st} bus, pertaining to the point 150

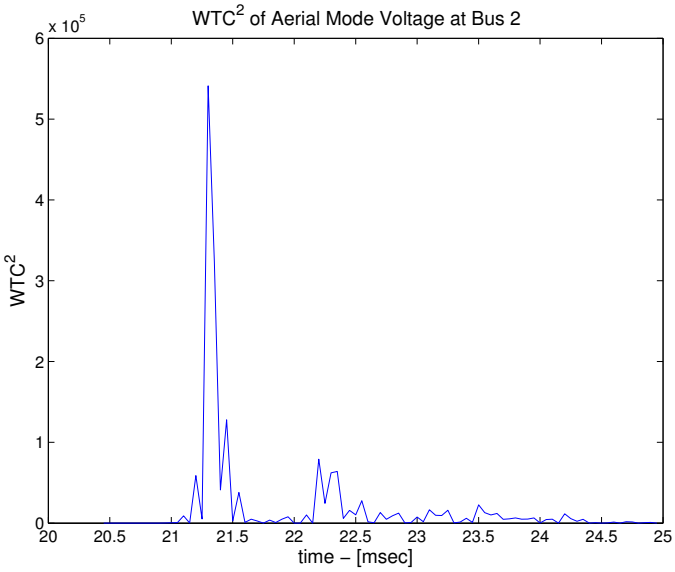

Fig. 7. WTC^2 of the aerial mode voltage at Bus 2 for the studied fault.

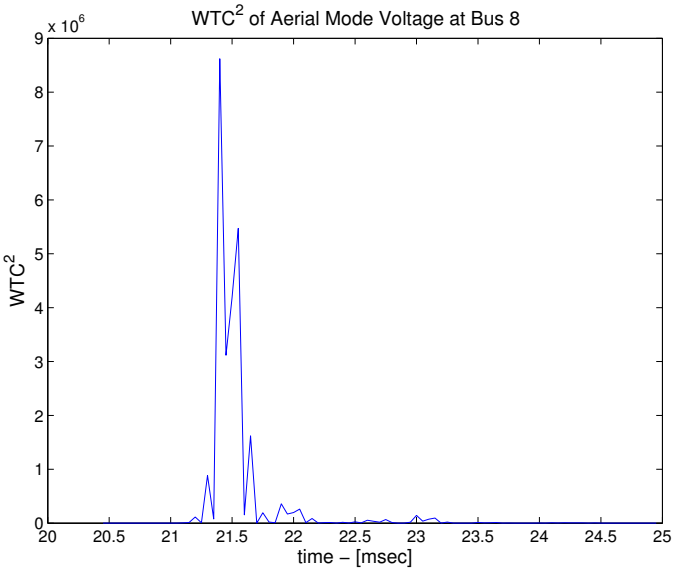

Fig. 9. WTC^2 of the aerial mode voltage at Bus 8 for the studied fault.

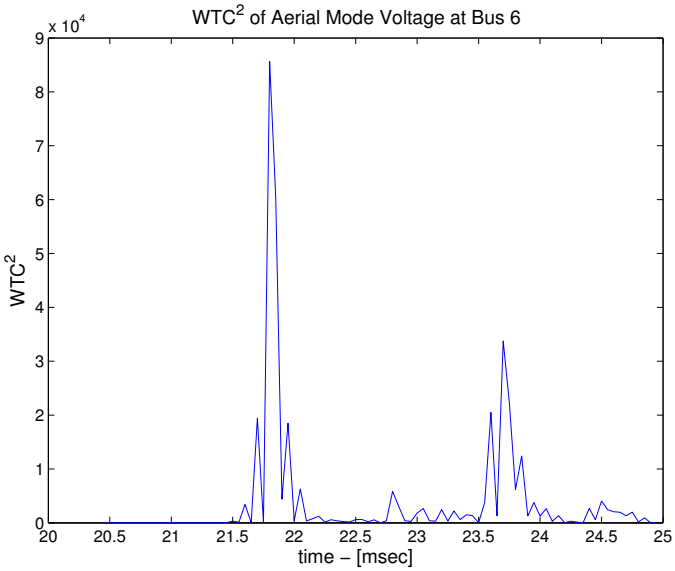

Fig. 8. WTC^2 of the aerial mode voltage at Bus 6 for the studied fault.

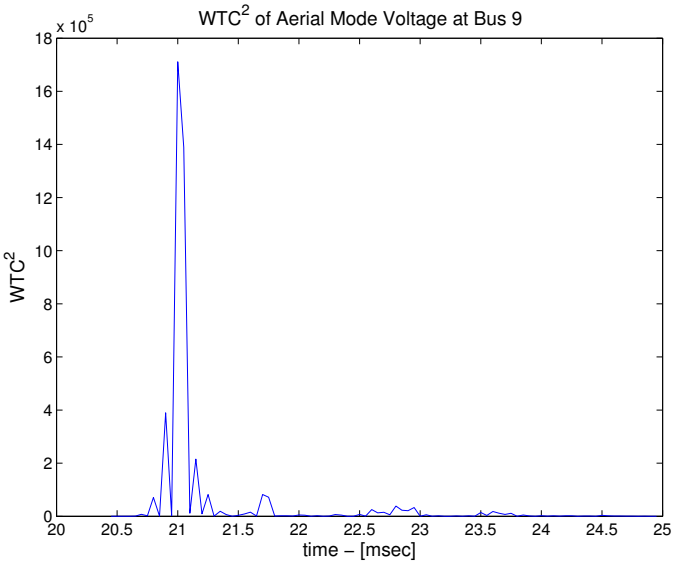

Fig. 10. WTC^2 of the aerial mode voltage at Bus 9 for the studied fault.

miles away from Bus 4 in the artificial network as shown in the following:

$$\widehat{\boldsymbol{\mathcal{T}}}_{\mathbf{131}} = \begin{bmatrix} 1.2642 - 0.9415 \\ 1.7484 - 0.9415 \\ 1.3718 - 0.9415 \\ 1.9098 - 0.9415 \end{bmatrix} = [0.3227,\ 0.8069,\ 0.4303,\ 0.9683]^{\mathrm{T}},$$

with

$$\Delta\boldsymbol{\mathcal{T}}_{\mathbf{131}} = \boldsymbol{\mathcal{T}}^{\mathbf{T}}_{\mathbf{meas}} - \widehat{\boldsymbol{\mathcal{T}}}^{\mathbf{T}}_{\mathbf{131}} = [-0.0227,\ -0.0069,\ -0.0303,\ 0.0317],$$

yielding the minimum norm $\|\Delta\boldsymbol{\mathcal{T}}_{\mathbf{131}}\|_1 = 0.0916 \approx 0$.

As a matter of fact, the norm of the difference above can be considered insignificant since the small mismatches between the measured and computed arrival time differences result from sampling errors.

In interconnected transmission networks, several identical shortest paths from the fault point are not commonly encountered. If such cases occur, employing more synchronized recorders assists in minimizing the likelihood of obtaining multiple solutions.

A. *Effect of Fault Resistance—R_f*

All the simulations are repeated substituting the fault resistance by $R_f = 250\ \Omega$. It is observed that the initial peaks of the square of aerial mode wavelet coefficients are smaller than those obtained by using very small fault resistance; however, the shape and peak arrival instants of the waveforms remain

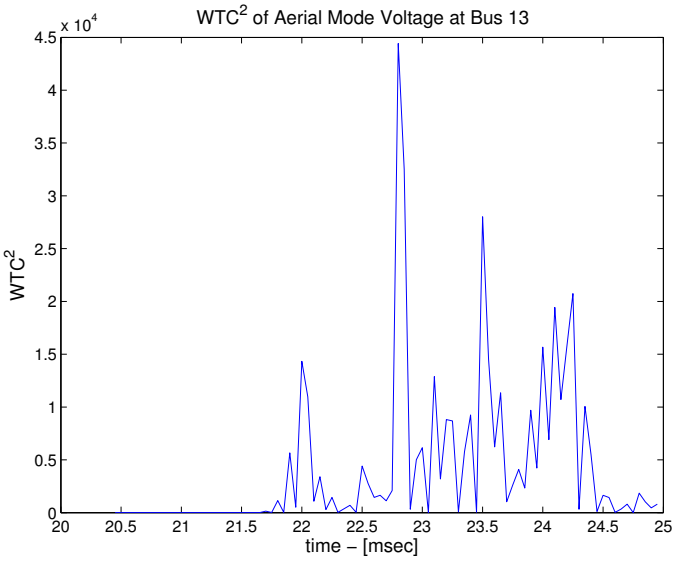

Fig. 11. WTC^2 of the aerial mode voltage at Bus 13 for the studied fault.

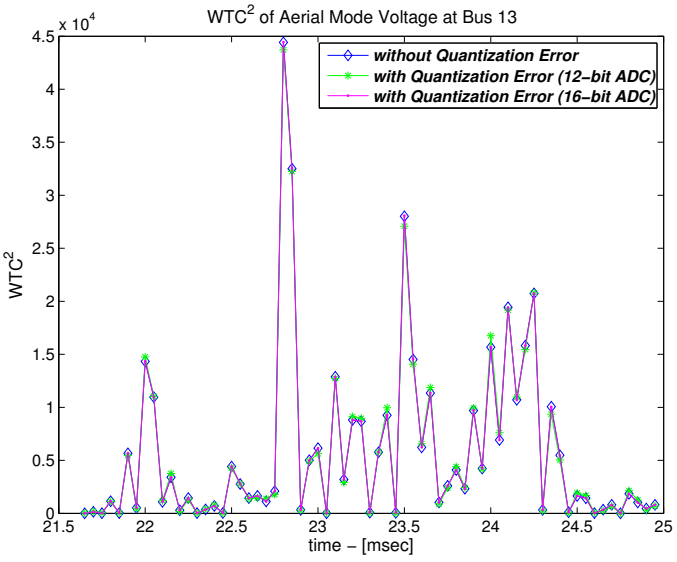

Fig. 12. WTC^2 of the aerial mode voltage at Bus 13 with and without quantization error.

the same. The fault location results produced by very small fault resistance match closely with those obtained with using 250-Ω fault resistance. Given this limited set of experimental results, it is anticipated that the algorithm performance will remain insensitive to variations in the fault resistance.

B. Effect of Quantization Error

It is worth pointing out that analog-to-digital converters (ADCs) used in representing analog signal with detailed digital representation are prone to errors, one of which is the quantization error. In this respect, simulations are repeated by introducing the random error to the simulated voltage signals. A zero-mean Gaussian noise is generated with standard deviation, σ, equal to the 35% of the quantization error ($0.35q$). In general, the fundamental formulation of the quantization error introduced by the ADC is given by [13]

$$q \triangleq 2^{-N} \times V, \tag{9}$$

where N is the number of the bits of the ADC and V is selected as the *maximum* value of the steady-state voltage signal.

Since 12- and 16-bit ADCs are the two widely commercially available converters, they can be chosen in investigating the effect of random errors arising from the quantization. It is inferred from the simulations that the magnitudes of the coefficients due to the random errors are negligible compared to the coefficients which are due to the fault-initiated transients, meaning that the quantization error has no impact on the first peak instants of the aerial mode WTC^{2}s as shown in Fig. 12. Also, one can evidently observe that the larger the number of bits in an ADC, the smaller is the quantization error. Therefore, accessibility to higher-resolution converters will undoubtedly contribute to further elimination of the existing insignificant effects of quantization errors.

C. Effect of Sampling Frequency—f_s

In order to demonstrate the effect of different sampling frequencies on the peak arrival instants of wavelet transform coefficients of the aerial mode voltages, simulations are carried out under various frequencies ranging from 10 kHz up to 1 MHz. Wave arrival times and calculated distances (in miles) to fault are given for different sampling frequencies in Tables II and III, respectively. The simulation results illustrated in Table II show that the accuracy of the fault location algorithm is proportional to the sampling frequency, i.e., the larger the sampling frequency, the more accurate the results. Moreover, although not illustrated visually, it is observed that the magnitudes of WTC^{2}s increase as the sampling frequency decreases.

TABLE II
WAVE ARRIVAL TIMES (IN MILLISECONDS) WITH RESPECT TO SAMPLING FREQUENCIES

f_s	t_2	t_6	t_8	t_9	t_{13}
1 MHz	21.2660	21.7500	21.3760	20.9480	21.9380
500 kHz	21.2640	21.7520	21.3720	20.9440	21.9400
200 kHz	21.2600	21.7500	21.3700	20.9400	21.9400
100 kHz	21.3100	21.7800	21.3900	20.9600	21.9600
50 kHz	21.3000	21.7600	21.4400	20.9800	21.9600
20 kHz	21.3000	21.8000	21.4000	21.0000	22.0000
10 kHz	21.4000	21.8000	21.4000	21.0000	22.0000

TABLE III
DISTANCE-TO-FAULT (DTF) VALUES (IN MILES) WITH RESPECT TO SAMPLING FREQUENCIES

f_s	$\mathbf{DTF_2}$	$\mathbf{DTF_6}$	$\mathbf{DTF_8}$	$\mathbf{DTF_9}$	$\mathbf{DTF_{13}}$
1 MHz	235.33	325.29	255.77	176.22	360.24
500 kHz	234.95	325.67	255.03	175.47	360.61
200 kHz	234.21	325.29	254.66	174.73	360.61
100 kHz	243.51	330.87	258.38	178.45	364.33
50 kHz	241.65	327.15	267.67	182.16	364.33
20 kHz	241.65	334.59	260.23	185.88	371.76
10 kHz	260.23	334.59	260.23	185.88	371.76

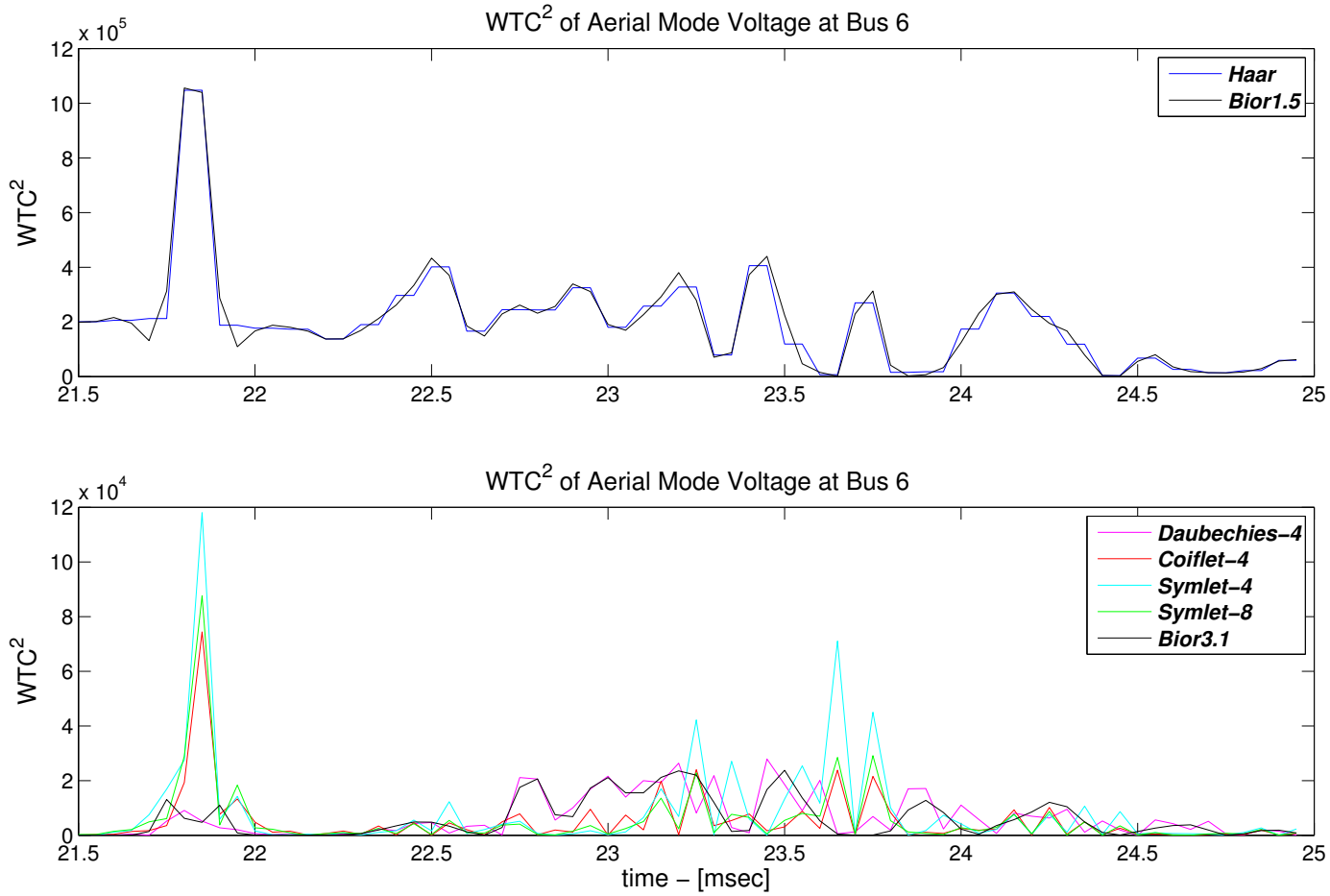

Fig. 13. WTC^2s of the aerial mode voltage at Bus 6 with different types of mother wavelets.

TABLE IV
MISCELLANEOUS MOTHER WAVELETS VERSUS WAVE ARRIVAL TIMES

MOTHER WAVELET	t_2	t_6	t_8	t_9	t_{13}
Haar	21.3000/ 21.3500	21.8000/ 21.8500	21.4000/ 21.4500	21.0000/ 21.0500	22.0000/ 22.0500
Daubechies − 4	21.3000	21.8000	21.3500	21.0500	22.1000
Coiflet − 4	21.3500	21.8500	21.4000	21.0500	22.0500
Symlet − 4	21.3500	21.8500	21.4500	21.0500	22.0500
Symlet − 8	21.3500	21.8500	21.4500	21.0500	22.0500
Bior1.5	21.3500	21.8000	21.4000	21.0000	22.0000
Bior3.1	21.2500	21.7500	21.4000	21.1000	22.0500

D. Effect of Mother Wavelet Selection

In order to illustrate the impact of the mother wavelet selection on the wave arrival instants, simulations are replicated using various wavelet families, such as Haar, Daubechies-4, Coiflet-4, Symlet-4, Symlet-8, and biorthogonal spline wavelets (*e.g.*, Bior1.5 and Bior3.1) since the DWT computation can be performed only with these wavelet bases. The results concerning WTC^2s of aerial mode voltage at Bus 6 are highlighted in Fig. 13 for the sake of illustration. Table IV lists the peak arrival instants of WTC^2s corresponding to different wavelet families.

IV. CONCLUDING REMARKS AND FURTHER STUDY

This paper presents a fault location procedure based on wide-area synchronized measurements for interconnected transmission networks. The procedure is based on processing of traveling waves by wavelet transform in order to extract the arrival times of fault-initiated waves reflected from the fault point. The proposed technique uses recorded samples of voltage waveforms whose data can be monitored at a few existing digital fault recorders in the system. The method is dependent on synchronized sampling, which can be ensured by utilizing conventional Global Positioning System (GPS) devices. Also,

it is assumed that the transient voltage waveforms are captured at a limited number of buses in the studied system. Increasing the number of measuring devices will definitely enhance the reliability of the fault location estimate. In the meantime, proposed procedure has the benefit of being able to identify the fault location properly using a small number of synchronized measuring devices. Furthermore, the results of this paper can be broadened to investigate the feasibility of installing these synchronized monitoring instruments at strategic locations as well as determining their optimal number.

ACKNOWLEDGMENT

This work is supported in part by the National Science Foundation under Grant No. ECCS-0824005. The authors would like to express their gratitude for this support.

REFERENCES

[1] F. H. Magnago and A. Abur, "Fault location using wavelets," *IEEE Trans. Power Del.*, vol. 13, no. 4, pp. 1475-1480, Oct. 1998.

[2] C. Y. Evrenosoğlu and A. Abur, "Travelling wave based fault location for teed circuits," *IEEE Trans. Power Del.*, vol. 20, no. 2, pp. 1115-1121, Apr. 2005.

[3] T. Nagasawa, M. Abe, N. Otsuzuki, T. Emura, Y. Jikihira, and M. Takeuchi, "Development of a new fault location algorithm for multi-terminal two parallel transmission lines," *IEEE Trans. Power Del.*, vol. 7, no. 3, pp. 1516-1532, Jul. 1992.

[4] A. A. Girgis, D. G. Hart, and W. L. Peterson, "A new fault location technique for two- and three-terminal lines," *IEEE Trans. Power Del.*, vol. 7, no. 1, pp. 98-107, Jan. 1992.

[5] Q. Gong, Y. Chen, C. Zhang, and Z. Wang, "A study of the accurate fault location system for transmission line using multi-terminal signals," *IEEE PES Winter Meeting*, vol. 4, pp. 2533-2538, Jan. 2000.

[6] S. M. Brahma and A. A. Girgis, "Fault location on a transmission line using synchronized voltage measurements," *IEEE Trans. Power Del.*, vol. 19, no. 4, pp. 1619- 1622, Oct. 2004.

[7] K.-P. Lien, C.-W. Liu, C.-S. Yu, and J.-A. Jiang, "Transmission network fault location observability with minimal PMU placement," *IEEE Trans. Power Del.*, vol. 21, no. 3, pp. 1128-1136, Jul. 2006.

[8] C.-W. Liu, K.-P. Lien, C.-S. Chen, and J.-A. Jiang, "A universal fault location technique for N-terminal ($N \geqq 3$) transmission lines," *IEEE Trans. Power Del.*, vol. 23, no. 3, pp. 1366-1373, Jul. 2008.

[9] Z. Galijasevic and A. Abur, "Fault area estimation via intelligent processing of fault-induced transients," *IEEE Trans. Power Syst.*, vol. 18, no. 4, pp. 1241-1247, Nov. 2003.

[10] E. Clarke, *Circuit Analysis of AC Power Systems, Symmetrical and Related Components*. New York: John Wiley & Sons, 1943.

[11] I. Daubechies, *Ten Lectures on Wavelets*. Philadelphia, PA: SIAM, 1992.

[12] E. W. Dijkstra, "A note on two problems in connection with graphs," *Numerische Mathematik 1*, pp. 269-271, 1959.

[13] A. G. Phadke and J. S. Thorp, *Computer Relaying in Power Systems*, 2nd ed. New York: John Wiley & Sons, 2009.

Mert Korkalı (S'06) received the B.S. degrees in electrical and electronics engineering and in industrial engineering from Bahçeşehir Üniversitesi, Istanbul, Turkey, in 2008 and the M.S. degree in electrical engineering from Northeastern University, Boston, MA, in 2010. He is currently a Ph.D. student in the Department of Electrical and Computer Engineering at Northeastern University, Boston, MA.

His research interests revolve around state estimation in electric power systems and fault identification in transmission and distribution networks.

Ali Abur (F'03) received the B.S. degree from Orta Doğu Teknik Üniversitesi, Turkey, in 1979, the M.S. and Ph.D. degrees from The Ohio State University, Columbus, OH, in 1981 and 1985, respectively. He was a Professor at the Department of Electrical Engineering, Texas A&M University, College Station, from 1986 to 2005. Since November 2005, he has been a Professor and Chair of the Department of Electrical and Computer Engineering, Northeastern University, Boston, MA.

His research interests are in computational methods for the solution of power system monitoring, operation, and control problems.